2nd URSI AT-RASC, Gran Canaria, 28 May – 1 June 2018

High-Power Broadband Active Phased-Array Transmitter

Young-Pyo Hong[(1)] and Woosang Lee[(2)]
(1) Korea Research Institute of Standards and Science, Daejeon, 34113, South Korea
(2) Agency for Defense Development, Daejeon, 34060, South Korea

Abstract

This paper presents 2.5-6 GHz phased-array transmitter, which can be used to generate 1-kW peak pulsed output. It consists of 16×12 transmit modules and each transmit module with greater than 37.5 dBm of CW output power is attached to rigid tapered slot antenna. In transmit module, integrated multi-function corechip is designed in order to individually control both amplitude and phase of array antennas. Far-field radiation pattern of active phased-array transmitter was obtained using field-transformation method after carrying out near-field measurement in anechoic chamber. Electronic beam steering capability of active phase-array transmitter was demonstrated with a scan angle of $\pm 7^{o}$ in both azimuth and elevation angle. The overall system size is $620\times421\times771$ mm^3.

1. Introduction

Gallium nitride (GaN) phased-array transceivers have attracted considerable attention for modern military and commercial applications [1]-[3]. In particular, broadband beam-steering transceivers, one of the key challenges is how to realize constant time delay across the entire spectral bandwidth. Among various time-delay techniques, true-time delay (TTD) [4] beamforming is a promising approach to solve the well-known beam squint problem [5]. In this paper, CMOS-based TTD multi-function corechip (MFC) is designed in order to individually control both amplitude and phase of array antennas. TTD MFC is comprised of gain amplifier, 6-bit digital step attenuator (DSA) block, 6-bit TTD circuits, and serial digital interface with small chip size and flat group delay response. This allows for the construction of compact 2.5-6 GHz phased-arrays using standard PCB techniques at a great reduction in cost and boost in reliability using quad flat no-lead (QFN) packaging technique. Single-channel transmit module including power dividers, multi-stage MFC, multi-stage power amplifier, and radiating elements delivers an CW output power of more than 37.5 dBm.

Proposed phased-array transmitter is composed of 192-channel transmitter modules to achieve 1-kW peak pulsed output in the frequency range 2.5-6 GHz, and results in phased-array pattern scanning to ±7◦ in both azimuth-axis and elevation-axis. Dummy radiating elements are placed on the edge of the active antenna array to compensate for mutual coupling in antenna arrays.

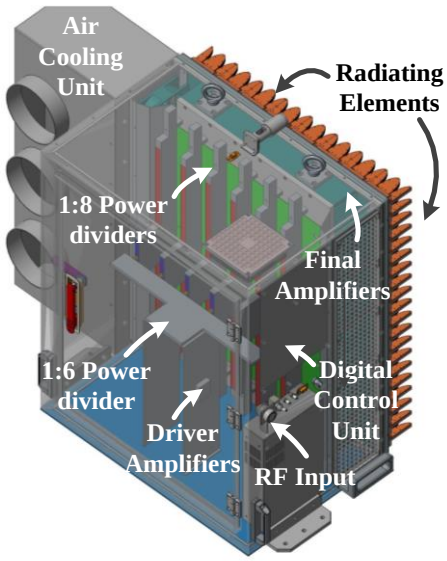

Figure 1. Active phased-array transmitter

2. Phased-Array Transmitter Design

The 3-dimentional view of phased-array transmitter architecture is shown in Fig. 1. The transmit module consists of power dividing networks, multi-function corechip (not shown in Fig. 1), driver amplifiers, final power amplifiers, digital control unit, and air cooling unit.

In particular, MFC composed of true time delay (TTD) and variable attenuator to provide phase control and amplitude control. In overall, the input signal is converted to four output signals and each output signal is attached to single antenna. Fabricated MFC is designed with TSMC 0.13-μm CMOS process. The TTD circuit is composed of SPDT/DPDT switches and time delay elements while DSA is implemented with the switched shunt resistor and a shunt switch transistor. To obtain low residual and quantization phase errors to support low side-lobe performance, 6 bits are used in the digital phase shifter (corresponds to TTD) MMIC within the transmit module.

Single-channel transmit module comprises multi-stage MFC, multi-stage amplifier (gain-block, drive amplifier, final PA) to obtain the output power (greater than 37.5 dBm) for the broadband antenna arrays. Individual RF components are packaged separately and they are all

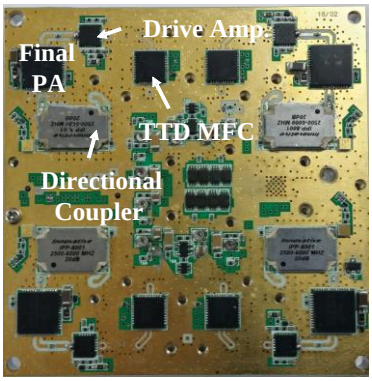

(a)

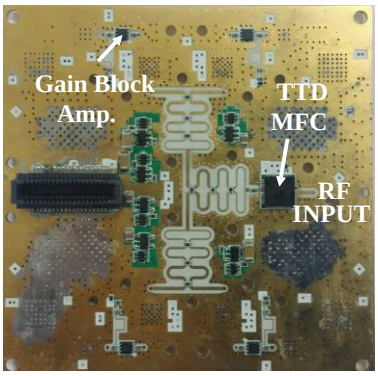

(b)

Figure 2. Four-channel transmit modules on the printed circuit board (a) top side (b) bottom side (PCB size: 74.3 mm^2).

TABLE I. SUMMARY OF TTD MFC PERFORMANCE

	Measured Results
Frequency Range	2.5 ~ 6.0 GHz
Gain	10 dB
P_{1dB}	7 dBm
# of delay bits	6 bits
Delay step	3.125 ps
# of attenuation bits	6 bits
Attenuation step	0.5 dB

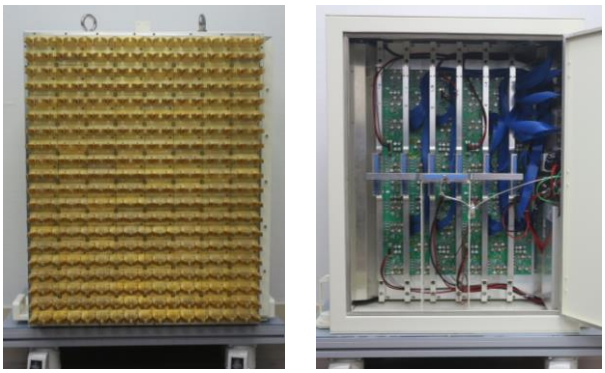

(a) (b)

Figure 3. Active phased-array transmitter (a) front view (b) rear view (system size: 620×421×771 mm^3).

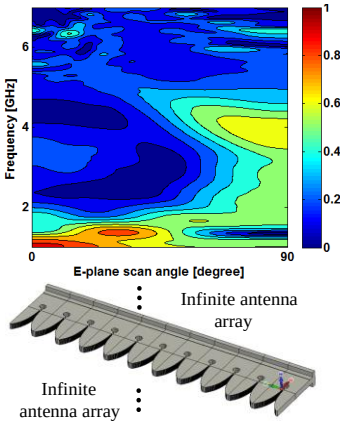

(a)

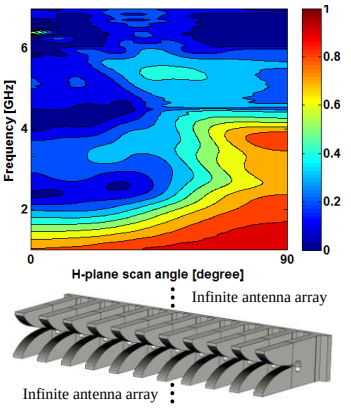

(b)

Figure 4. Simulated active reflection coefficient of the antenna array [unit: linear magnitude]: (a) *E*-plane and (b) *H*-plane

attached to a common 7.3-mil RO4350BTM substrate. Fig. 2 shows both top and bottom side of four-channel transmit modules fabricated on the printed circuit board.

MFC is used in all single-channel transmit modules. The measured results of MFC are summarized in Table I. The multi-stage amplifier section consists of drive amplifier (TriQuint's TGA2597-SM), and GaN MMIC power amplifier (Hittite's HMC1087). The host incorporates the RF manifold, DC distribution and logic/control distribution and is inserted into the active antenna array unit as a rack-mounted sub-assembly. In addition, forced-air cooling solution is used for active phased-array transmitter. Fig. 3 shows both front and rear view of active phased-array transmitter.

3. Simulated Results of the Array Antennas

Rigid tapered slot antennas are chosen as the array elements. As is well known, grating lobes are a consequence of the periodicity of the array pattern and depend on the distribution of the elements, and the maximum scanning angle arises when using a two-dimensional phased array. Therefore, the lattice configuration is very important to avoid the appearance of

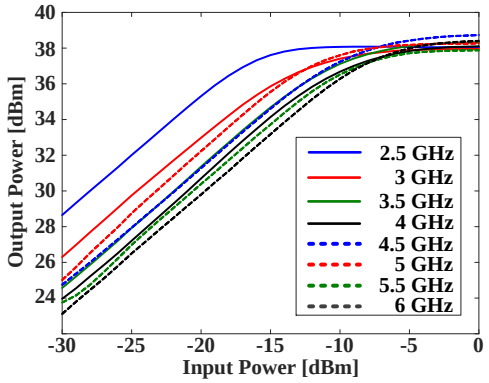

Figure 5. Measured output power for single-channel transmit module.

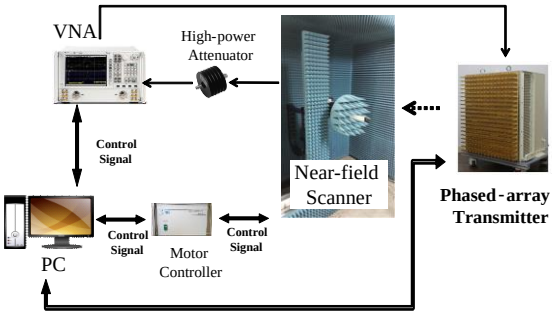

Figure 6. Near-field measurement setup.

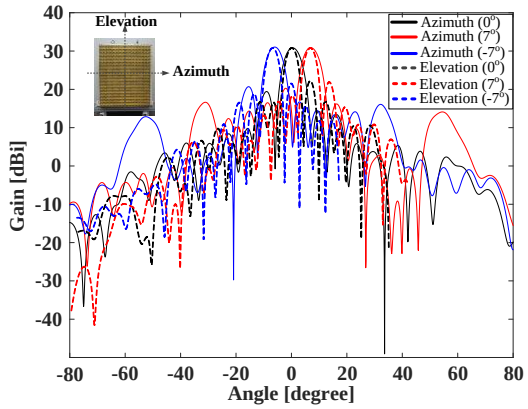

Figure 7. Transformed far-field radiation pattern from measured near-field data at 6 GHz.

grating lobes (except for the main lobe) within the visible space [6]. The lattice dimensions of the 192-element rectangular planar arrays are dx=dy=37.25 mm (dx corresponds to any two adjacent elements in the horizontal direction of array and dy corresponds to any two adjacent elements in the vertical direction of the array) to circumvent the grating lobes of the antenna array. In addition, the optimal lattice configuration is determined by considering the space for a mechanical connection between the antenna arrays and the transmit modules with a thermal management unit.

Each radiating element has an active reflection coefficient which varies with the scan angles. In Fig. 4, the simulated active reflection coefficient on both the *E*-plane and the *H*-plane when the array is radiating with different scan angles is shown. For the efficient electromagnetic simulation of large arrays, a two-dimensional antenna array with eleven elements in the horizontal direction and an infinite array in the vertical direction is modelled and simulated instead of total 192 element arrays. Fig. 4 shows that the mutual coupling has a pronounced effect on the performance with an increase in the scan angle resulting in a higher active reflection coefficient.

4. Measurement Results of the Transmitter

Measured output power versus input power for one of the transmit modules is plotted in Fig. 5 over subset of frequencies. The observed compression curves are well behaved with no evidence of kink or undesired oscillation. Saturated CW output power is greater than 37.5 dBm from 2.5 GHz to 6 GHz. The measurements with phased-array transmitter were performed in the near field facility. An overview of the test setup is shown in Fig. 6. All measurement system is automated and fully PC-controlled to obtain very large amounts of near-field data with high accuracy. A laser tracker is used to monitor the probe aperture location and the center of rotational positioning is reference to the phase center of the antenna. The simplest RF subsystem consists of source (vector network analyzer with pulsed-RF measurement option) which also serves as the receiver. Also a high-power attenuator between the source and phased-array transmitter is used for RF leveling and motor controller is necessary for mechanical movement of near-field scanner.

The amplitude and phase data are collected at known locations on the measurement surface. The near-field data set for a phased-array transmitter is utilized to accurately extract its far-field radiation patterns by a field transformation method [7]. Fig. 7 shows far-field radiation pattern for main beam directions of -7°, 0°, and 7° at 6 GHz along with azimuth- and elevation-axis.

4. Conclusions

The design and performance of a 2.5–6 GHz active-phased array transmitter has been presented. Single-channel transmit module delivers a CW output power of higher than 37.5 dBm, and results in 1-kW peak pulsed output power of active phased-array transmitter in entire operational frequency. Electronic beam steering capability of transmitter was successfully demonstrated with a scan angle of $\pm 7^{o}$ in both azimuth and elevation angle.

5. References

1. E. Brookner , “ Radar and phased array breakthroughs ,” *Microw. J.* , vol. 58 , no. 11 , pp. 20 – 37 , November 2015.

2. Y. S. Noh, I. B. Yom, "Highly Integrated C-Band GaN High Power Amplifier MMIC for Phased Array Applications", *IEEE Microw. Wireless Compon. Lett.*, vol. 25, pp. 406-408, April 2015.

3. D. Kim, D. H. Lee, S. Sim, L. Jeon, S. Hong, "An *X*-band switchless bidirectional GaN MMIC amplifier for phased array systems", *IEEE Microw. Wireless Compon. Lett.*, vol. 24, pp. 878-880, September 2014.

4. Q. Ma, D. M. W. Leenaerts, P. G. M. Baltus, "Silicon-based true-time-delay phased-array front-ends at Ka-band", *IEEE Trans. Microw. Theory Tech*., vol. 63, no. 9, pp. 2942-2952, September 2015.

5. R. J. Mailloux, *Phased Array Antenna Handbook*, 2nd ed. Norwood, MA, USA: Artech House, 2005.

6. S. R. Zinka, I.-B. Jeong, J.-H. Chun, J.-P. Kim, "A novel geometrical technique for determining optimal array antenna lattice configuration", *IEEE Trans. Antennas Propagat.*, vol. 58, no. 2, pp. 404-412, July 2010.

7. Y.-P. Hong, D.-J. Lee, N.-W. Kang, H. J. Koo, "Phase-stabilized W-band Planar Imaging System for Near-to-Far-field Projection based on Photonic Sensors", *IEEE Antennas and Wireless Propagat. Lett.*, (Accepted).